



ELSEVIER

Contents lists available at ScienceDirect

## Journal of Computational Physics

www.elsevier.com/locate/jcp



# Computational modeling of cardiac hemodynamics: Current status and future outlook



Rajat Mittal<sup>a,\*</sup>, Jung Hee Seo<sup>a</sup>, Vijay Vedula<sup>a</sup>, Young J. Choi<sup>a</sup>, Hang Liu<sup>b</sup>,  
H. Howie Huang<sup>b</sup>, Saurabh Jain<sup>c</sup>, Laurent Younes<sup>c</sup>, Theodore Abraham<sup>d</sup>,  
Richard T. George<sup>d</sup>

<sup>a</sup> Mechanical Engineering, Johns Hopkins University, United States

<sup>b</sup> Electrical and Computer Engineering, George Washington University, United States

<sup>c</sup> Applied Mathematics and Statistics, Johns Hopkins University, United States

<sup>d</sup> Division of Cardiology, Johns Hopkins University, United States

## ARTICLE INFO

### Article history:

Received 5 February 2015

Received in revised form 30 September 2015

Accepted 9 November 2015

Available online 17 November 2015

### Keywords:

Hemodynamics

Computational fluid dynamics

Cardiac physics

Blood flow

Cardiovascular disease

Heart disease

Cardiac surgery

Left ventricular thrombosis

Heart murmurs

Cardiac auscultation

Image segmentation

Immersed boundary methods

## ABSTRACT

The proliferation of four-dimensional imaging technologies, increasing computational speeds, improved simulation algorithms, and the widespread availability of powerful computing platforms is enabling simulations of cardiac hemodynamics with unprecedented speed and fidelity. Since cardiovascular disease is intimately linked to cardiovascular hemodynamics, accurate assessment of the patient's hemodynamic state is critical for the diagnosis and treatment of heart disease. Unfortunately, while a variety of invasive and non-invasive approaches for measuring cardiac hemodynamics are in widespread use, they still only provide an incomplete picture of the hemodynamic state of a patient. In this context, computational modeling of cardiac hemodynamics presents as a powerful non-invasive modality that can fill this information gap, and significantly impact the diagnosis as well as the treatment of cardiac disease. This article reviews the current status of this field as well as the emerging trends and challenges in cardiovascular health, computing, modeling and simulation and that are expected to play a key role in its future development. Some recent advances in modeling and simulations of cardiac flow are described by using examples from our own work as well as the research of other groups.

© 2015 Elsevier Inc. All rights reserved.

## 1. Introduction

Among all diseases, cardiovascular disease (CVD) remains the leading cause of mortality (about 33%) in the US. In 2012, the incidence of CVD in adults aged  $\geq 20$  years was 35% and about 800,000 deaths were attributed to CVD [1]. While improvements in diagnosis and treatment have led to improved outcomes and reduced rate-of-mortality since the 1970s, other trends associated with CVD point to a troubling future (see Fig. 1(a)). CVD has a strong correlation with age and by 2050, more than 40% of the population (about 200 million adults) will be  $\geq 45$  years old. Heart disease also has a positive correlation with obesity and since 1980, the percentage of adults aged 20–74 who are considered clinically obese, has doubled to more than 30% [1]. CVD also has a positive correlation with diabetes, the incidence of which is also growing

\* Corresponding author.

E-mail address: mittal@jhu.edu (R. Mittal).

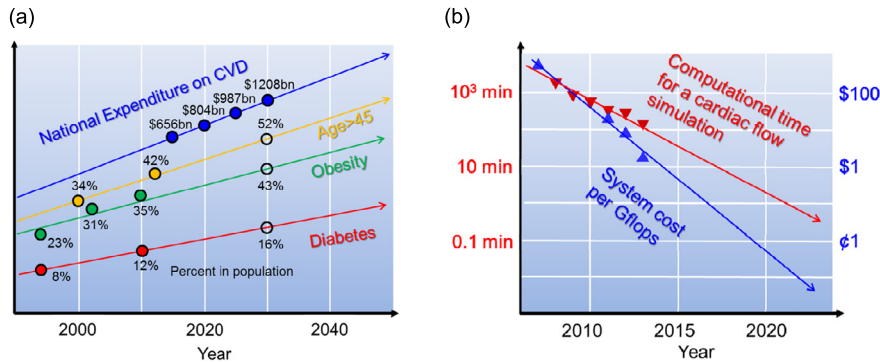


**Fig. 1.** (a) Trends in the cardio vascular disease [1], <http://www.census.gov/population/age/>. (b) Trends in computational speed and cost with time. Computational time for a cardiac simulation is estimated for a simulation with 25 million grid points which requires approximately 1 ExaFLOP on a world #500 cluster (<http://top500.org/statistics/perfdev/>). System cost per a Gflops is based on <http://en.wikipedia.org/wiki/FLOPS>.

steadily with time. Additionally, CVD ranks highest in terms of national healthcare expense with close to half a trillion dollars spent on this in 2010; this is more than twice the health expenditures on cancer, which is the next most expensive disease [1]. The high healthcare cost of CVD is due not only to its prevalence in the population, but also to the cost of the treatment; the mean hospital charge for a CVD procedure was close to sixty thousand dollars in 2010 [1] and these costs are projected to rise faster than the cost-of-living in the foreseeable future. While the numbers reported here are for the US, the trends are not very different for the world population at large. Many of these costs result from under-treatment or over-treatment and often a reliance on costly invasive procedures that may or may not improve downstream outcomes.

Thus, improvements in diagnosis and the guidance of proper therapies (medical and/or invasive) are required to deliver cost-effective treatments to patients. However, many examples are available where outcomes may be improved in some, but not all patients by using technology that is very expensive. For example, cardiac resynchronization therapy with biventricular pacemakers aimed at improving cardiovascular hemodynamics, is a costly therapy that results in approximately 11–46% of the recipients deriving no benefit [2]. In the case of CVD that alters cardiac hemodynamics, the only way to tackle this burgeoning crisis is to develop technologies that accurately characterize cardiac hemodynamics and enable better selection of patients for costly invasive versus less costly medical therapies. The key is to develop technologies that improve treatment outcomes without concurrently increasing the cost of diagnosis and treatment.

One way to tip the scales in our favor is to counteract these unfavorable trends with ones that are favorable, and one trend that is significantly in our favor is the Moore's Law [3], which refers to the trend in computing, enabled by increases in clock-speed, concurrency, memory and memory bandwidth, that has continuously enabled ever-larger, faster and cheaper computations. Some of the largest supercomputers today reach speeds in the PFLOPS (Peta Floating-point Operations per Second) but a thousand-fold increase to  $10^{18}$  FLOPS or ExaFLOPS (EFLOPS) is expected in less than 10 years. In addition to the speed of computation, the cost of computation is also an important factor when considering applications to medical therapy and diagnostics. In this regard, it has been noted that the cost per FLOP has also been cut by roughly 50% each year; a trend which is also expected to continue into the future (Fig. 1(b)). Commoditization of computational resources through virtualization and cloud-computing will further accelerate cost reductions and make high-performance computing ubiquitous.

From the point-of-view of computational modeling, it is useful to separate cardiovascular hemodynamics into cardiac hemodynamics (blood flow in the left and right ventricles and atria of the heart) and vascular hemodynamics (blood flow in the vessels that transport blood to and from these chambers to the rest of the body). The latter, i.e. computational modeling of vascular hemodynamics is a relatively mature field especially for larger vessels that are well resolved by medical imaging (e.g. aorta and main branches of coronary arteries). The simulations of blood flow in these larger vessels are becoming more reliable by coupling with lumped elements models [4,5] of the circulatory system and the smaller vessels. There are numerous examples where such modeling has either reached or will soon reach translation to clinical applications [6,7]. An excellent example in this regard is the CFD-based protocol for the assessment of the functional significance of coronary artery stenoses developed by HeartFlow [7], which recently been approved by FDA for clinical use. Other examples in vascular hemodynamics, where CFD modeling has advanced significantly towards clinical application include optimization of the Fontan procedure [8,9] and treatment of Kawasaki disease [10].

The current article, however, focuses on computational modeling of *cardiac* hemodynamics, i.e. the flow in the chambers of the heart (see Fig. 2), which presents some different challenges for computational modeling and which, due to these challenges, is further away from clinical application. These challenges are primarily due to the large-scale motion and complex deformation of the chambers (the LV for instance changes its volume by almost 100% of the end-systolic volume in every cardiac cycle), complex flow-induced dynamics of the valves and a higher flow Reynolds number which induces transition to turbulence.

The present article is organized as the following. In section 2, the potential clinical applications of cardiac simulations and the required computational performance is discussed. In section 3, the recent advances in cardiac simulation and the

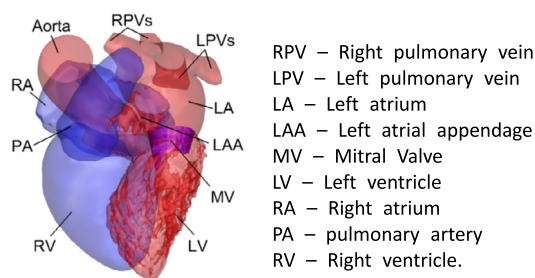


**Fig. 2.** Key anatomical features of the cardiac chambers of the human heart. Figure shows the cardiac lumen extracted from a contrast-enhanced cardiac CT scan.

key challenge for the patient-specific simulation are described. The approach to patient-specific cardiac simulation taken by our group is briefly described in section 4, simulation results and multiphysics modeling methods highlighted in section 5. In section 6, we describe our experience and approach to GPU acceleration of cardiac simulations, and concluding remarks are provided in section 7.

## 2. Clinical applications

Simulating heart function through physics-based models is an obvious way in which the power of the Moore's law can be brought to bear on the treatment of heart disease. Most cardiac diseases (such as cardiomyopathies, valvular disease, congenital heart disease, and arrhythmias) either originate in the heart or manifest through their effect on heart function. As such, computational models that enable a better fundamental understanding of cardiac dynamics (electrophysiology, mechanics and hemodynamics) in normal as well as diseased hearts could significantly advance the diagnosis and treatment of heart disease. Simulation-enhanced diagnostics and simulation-guided surgical planning and therapy could also directly lead to improved outcomes and reduced costs. Take for example the surgical management of hypertrophic obstructive cardiomyopathy (HOCM) [11], a leading cause of sudden cardiac death in otherwise healthy individuals, and a condition that causes significant morbidity in patients with advanced forms of the disease. HOCM is a condition where the thickening of the myocardium of the left ventricle (LV) obstructs blood flow into the aorta during systole. The obstruction of the LV outflow tract is dynamic and can be dependent on preload and afterload conditions. In addition, low pressure in the outflow tract during systole can lead to flow-induced systolic anterior motion (SAM) of the mitral valve leaflets resulting in massive regurgitation across the mitral valve leaflets and reduction or even cessation of flow to the aorta. Typical therapies for HOCM include surgical myectomy (surgical removal of the hypertrophic obstruction), and/or mitral leaflet plication [12]. Each of these options has its risks and benefits, and the surgeon relies on imaging (echocardiography and Doppler ultrasound) as well as experience to choose a particular therapy for a given patient. However, the complex hemodynamics in the outflow tract coupled with flow-induced leaflet dynamics can make the effect of such a surgery difficult to predict even for an experienced surgeon. In such a scenario, a patient-specific, hemodynamic model of the heart could empower the surgeon in choosing the most effective therapy, thereby improving patient outcome, and reducing costly revisions. In addition to HOCM, cardiac hemodynamic models could assist with the surgical planning of heart transplants, ventricular assist devices (VAD) [13], implantation of prosthetic valves [14], valve repair (e.g. mitral clip surgery) [15] and cardiac-resynchronization therapy (CRT) [16].

Cardiac simulations can also be used to enhance existing diagnostic modalities. Two-dimensional echocardiography ("Echo") coupled with Doppler ultrasound has become the standard of care in managing structural heart disease and more recently CMR (Cardiac MRI) and 3D/4D echo are being more widely utilized. However, these imaging modalities continue to provide limited information regarding cardiac function and the diagnosis utilizes only a small fraction of the information that is available from these modalities. Cardiac hemodynamic models that incorporate X-ray computed tomography (CT), CMR or Echo information could provide information regarding flow patterns, blood residence time and flow stasis [17–25] that far exceed what is available from structural imaging alone, and in doing so, enhance the diagnostic value of these expensive procedures. An interesting example of such an approach can be found in [26]. Cardiac simulations can also non-invasively provide measures of quantities such as local pressures gradients, velocities and shear stress which can normally be obtained only through invasive procedures such as catheterization [27,28]. Applications of the above extend to a wide range of heart diseases including cardiomyopathies, diastolic dysfunction, valvular disease, myocardial infarction, atrial fibrillation, congenital heart disease and congestive heart failure. Multiphysics simulations that couple cardiac hemodynamics with other physics such as biochemistry, structural dynamics, and acoustics, further extends the application of simulation based diagnosis. For example, a coupled hemodynamics and coagulation biochemistry simulation can be used for the diagnosis and analysis of the left ventricular thrombus (LVT) formation in patients with myocardial infarction (MI) [29]. A coupling of the hemodynamics to the acoustic/structural wave propagation so as to simulate the generation and propagation of heart sounds could be applied to gain insights into the biophysics of cardiac auscultation.

While simulation of cardiac hemodynamics in *real-time* would open up unparalleled possibilities for point-of-care diagnostics and therapy, the vast majority of the applications described above become viable even with much longer computa-

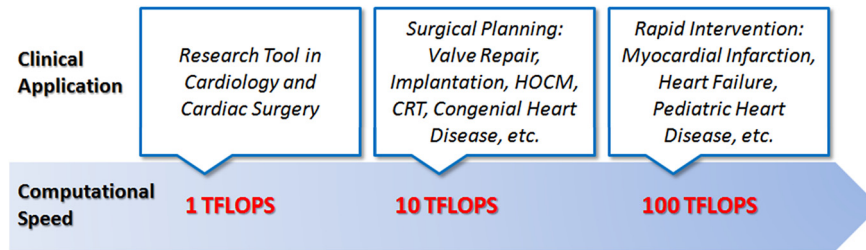


Fig. 3. Applications of cardiac simulation for available computational speeds.

tional turn-around times. Fig. 3 shows for the type of computation-based therapies that become available with increasing computational speeds. Conditions needing rapid intervention such as myocardial infarction, heart failure and some pediatric heart conditions might necessitate computational models that can be turned around in a few hours; this is equivalent to simulating at a speed 10,000X slower than real-time, and for a LV simulation, corresponds to a computational speed of about 100 TFLOPS. For applications such as valve repair or implantation, heart assist device implantation, HOCM, CRT as well as some congenial heart diseases, the planning stage for surgery extends over many days or weeks and therefore, a simulation for these conditions could be turned around in the order of a day; this is equivalent to 100,000X slower than real-time and a computational speed of 10 TFLOPS. As shown in Fig. 1, such computational speeds are eminently realizable in the next few years and at a cost that would make them a viable addition to the toolbox of interventional cardiologists, electrophysiologists, and cardiac surgeons. Finally, CFD can become a powerful research tool in cardiology and cardiac surgery if researchers can simulate a number of cases sufficient for computing reliable statistics and conducting comparative studies. A complete simulation every 10 days (which would give about 36 simulations per year of study) would be a good starting point and this requires a computational speed of about 1 TFLOPS.

### 3. Challenges and recent advances in cardiac simulation

As discussed in the previous sections, simulation-based diagnoses and therapies for heart conditions are around the proverbial corner; unleashing the potential of these therapies however, requires that modeling approaches and software tools keep pace with advances in computational hardware. Also, appropriate and efficient procedures are needed for translating information and data acquired for a patient into a CFD model as well as for the subsequent analysis of the simulation data.

The first challenge in the simulation of cardiac hemodynamics is the construction of patient-specific time-dependent cardiac models. One widely used approach is direct segmentation of time-dependent medical imaging data such as 4D CT/Echo and CMR to reconstruct a kinematic model of the heart. Although the segmentation and reconstruction of the patient specific cardiac motion is, in principle, relatively straight-forward, issues associated with the temporal/spatial resolution of the image create complications in this step of the model development procedure. Some of these are discussed later in this section. The other approach is to employ heart function models that incorporate biophysical modeling of cardiac electromechanics [30,31]. One good example of this approach is the “Living heart project” [32] where the excitation and contraction of four chambers of a human heart are simulated based on the electro-mechanical modeling. Although in the initial model [32], the flow component is simplified with a lumped element type model, it is possible to perform fully coupled electromechanics and hemodynamic simulations. Recent advances in the multi-scale electro-mechanical modeling [33] of myocardial tissues and advanced medical imaging such as a diffusion tensor MRI [34] which captures the fiber orientations, would enable such fully coupled simulation of cardiac motion and hemodynamics [35]. The advantage of such approaches is that the interactions between the cardiac electromechanics and cardiac flow can be investigated via first-principles. For example, McCormick et al. [36,37] investigated the effect of LVAD on the LV structure and hemodynamics using the coupled FSI simulations (see Fig. 4). Another recent example of a one-way coupled model is that of Choi et al. (2015) [35] which coupled a detailed multiscale model for cardiac electromechanics with a Navier–Stokes model for the hemodynamics, and used it to examine the effect of heart failure and dyssynchrony on LV hemodynamics. However, obtaining information (such as fiber orientation) for these models is costly, time consuming, and is currently based on data obtained post-mortem. Thus, implementation of these models within a clinical setting is currently not possible. It is however interesting to note that new methods [31] have proposed to transform a template fiber orientation data to patient-specific configurations, which could make a patient-specific cardiac function simulation more feasible. In the present paper, we focus on the direct image-based hemodynamic modeling approach and the procedures and challenges associated with this approach are discussed below.

Fig. 5 shows a flowchart describing the typical steps in conducting an imaging-based patient-specific cardiac flow simulation. The procedure begins with obtaining patient-specific anatomical data for the heart via in-vivo medical imaging modalities such as Echo, MRI, or CT-scans. The cardiac images obtained from the medical imaging need to be segmented and registered to construct a three-dimensional, dynamic (moving) model of the heart for the flow simulation. The dynamic 3D model should have adequate spatial as well as temporal resolution and this is the first challenge in patient-specific cardiac flow simulation. 4D-Echo (three space dimensions and time) provides high temporal resolution (30–100 Hz) which is particularly useful when resolving the rapid movements of structures such as valve leaflets. However, the lower spatial resolution and image quality of this modality make it difficult to clearly resolve fine scale features such as ventricular

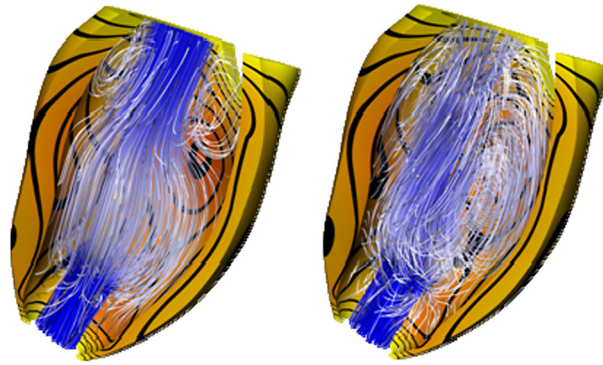


**Fig. 4.** An example of coupled heart function simulation. Investigation of diastolic filling in the left ventricle under left ventricular assist device support. Left to right shows instantaneous streamlines and wall motion at intermediate time points through the filling phase. Streamlines are colored white to blue indicating increasing velocity magnitude. The myocardial wall is colored yellow to red with equally spaced contour bands illustrating displacement magnitude. (Image provided by Dr. David Nordsletten.) (For interpretation of the references to color in this figure legend, the reader is referred to the web version of this article.)

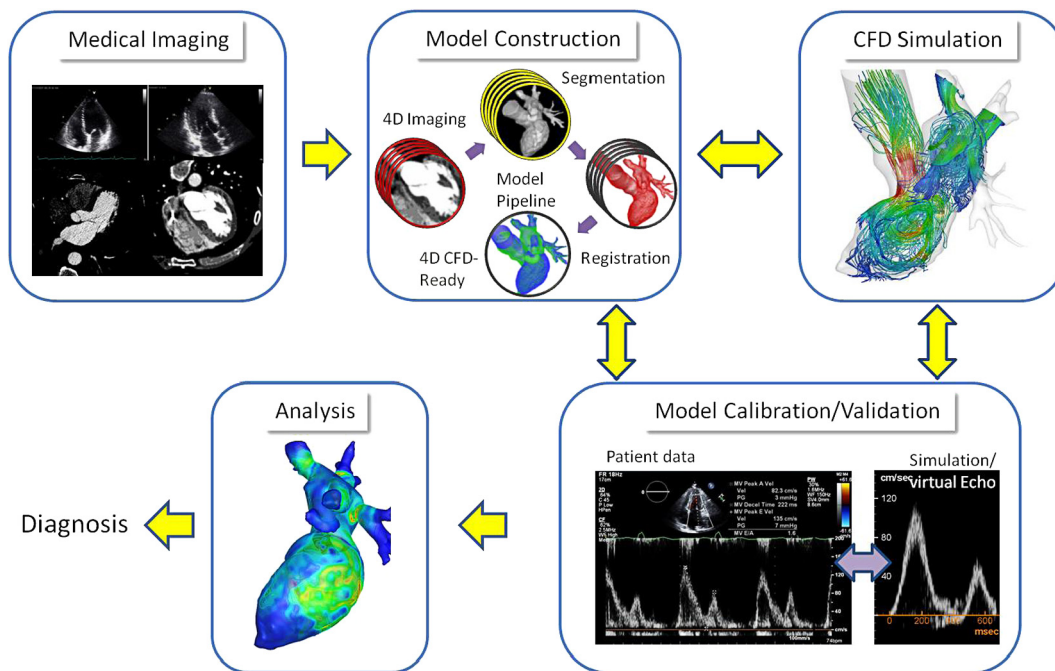


**Fig. 5.** Pipeline for conducting patient-specific cardiac flow simulations.

trabeculae. Modalities such as CMR and Cardiac CT on the other hand, provide excellent spatial resolution. CMR has an in-plane resolution of  $1.5 \times 1.5$  mm, but more limited through-plane resolution (typically about 8 mm) while CT is capable of isotropic spatial resolution on the sub millimeter scale ( $\sim 0.5$  mm) and clear delineation of trabeculae and lumen boundaries. CMR has the advantage of higher temporal resolution (30–50 ms) while temporal resolution in CT depends on the scanning system (50–200 ms). This is orders-of-magnitude lower than the temporal resolution required for the flow simulation ( $\sim 1000$  phases per cardiac cycle) and appropriate interpolation methods need to be employed to create CFD-ready models. This stage of model generation has been very difficult to automate, and remains the biggest bottleneck for patient-specific cardiac flow modeling.

Once the time-resolved, dynamic 3D heart model has been constructed, the simulation of blood-flow is performed by applying the techniques of computational fluid dynamics (CFD). This is the most computationally intensive component of cardiac flow modeling and presents the second key challenge. This is particularly so because ventricular flows involve large volume change, flow transition at moderately high flow Reynolds number (about 4000), and interaction of flow with flexible structures. Depending on the need of the particular problem at hand, one or more of these features might have to be modeled accurately, thereby imposing significant modeling and/or computational requirements. In this context, immersed boundary methods (IBMs) offer a comprehensive simulation paradigm for such flows [22,25]. With the IBM approach, which

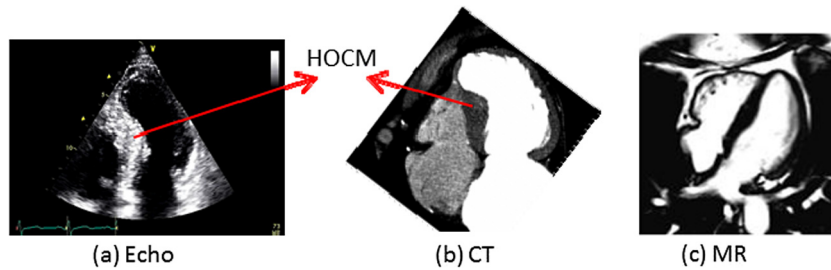


**Fig. 6.** (a) Apical three-chamber of a heart with hypertrophic obstructive cardiomyopathy (HOCM), obtained using echocardiography. (b) Four-chamber axial slice of the same heart obtained using 4D CT. Note that this figure has been rotated to facilitate direct comparison with the Echo image in (a). (c) Four-chamber view of normal human heart using 4D MRI.

are originally developed by Peskin for the very purpose of modeling cardiac hemodynamics [38–41], the dynamic 3D lumen of the model can simply be immersed into a Cartesian volume domain to perform the hemodynamic simulation on a structured Cartesian grid. Based on our own experience in modeling such flows, we estimate that in order to perform accurate simulation of flow in the left ventricle, grids ranging from 10–25 million points and time-steps per cardiac cycle ranging from 5,000–20,000 are required. As discussed above, in 2014, a complete computation of the LV with 25 million points takes about 80 hours using parallel computation with 512 CPU cores. Based on Moore's law however, this computational time may be reduced to less than an hour in 10 years (see Fig. 1(b)), and the simulations could be further accelerated by employing GPUs (Graphics Processing Units), which have thousands of processing cores and thus, yield better computational performance than CPUs. It is expected that the simulation of one cardiac cycle could be completed in several minutes using GPUs by 2020. The key in the transition from CPU computation to GPUs is the optimization of flow simulation algorithm for parallel computation employing  $O(10^6)$  processing cores and this is the third key challenge in this arena.

The hemodynamic data obtained from the flow simulation can be directly used to investigate the flow patterns as well as clinically important metrics such as pressure gradients, wall shear stresses (WSS), vortex propagation and residence times. In addition to these, the hemodynamic data can be synthesized to generate "virtual" cardiographic data such as that obtained from Doppler echocardiography (shown in Fig. 5 for example), phonocardiography, and ventriculography. These virtual cardiographies directly connect the computational fluid dynamics results with data from the clinical diagnostic modalities, and facilitate cardiac diagnosis. Virtual cardiographic data can also be used for rapid validation of a patient-specific cardiac flow simulation, as shown in Fig. 5. In this context, it is noted that although computational modeling and numerical methods for the cardiac flow simulations can be validated and verified against laboratory models, such validation/verification does not guarantee the accuracy of the computational result for a particular patient-specific model simulation. This is primarily because the patient-specific input data such as inflow/outflow conditions required for the simulation are oftentimes limited, and some of these need to be approximated or modeled. This can introduce errors in the simulation which have to be assessed prior to using the simulation data for diagnosis and treatment. The use of 'virtual' cardiography for validation can facilitate such rapid, in-clinic validation and the development of point-of-care validation protocols is another key challenge that needs to be addressed.

In the following sections, we describe our current efforts to develop a methodology that can provide rapid, patient-specific cardiac flow simulation in the near future by addressing the aforementioned challenges. As appropriate, we also briefly mention promising approaches that are being employed in this arena by other researchers as well as issues that remain unaddressed.

## 4. Patient-specific computational models of cardiac flows

### 4.1. Imaging modalities

For the patient-specific cardiac flow simulation, it is required to obtain the anatomical model of the patient's heart from noninvasive cardiac imaging such as echocardiography (Echo), magnetic resonance imaging (MRI), and computed tomography (CT) (Fig. 6). Each imaging modality has its own advantages and disadvantages associated with image quality, cost, speed, availability and invasiveness. Echo (which may be transthoracic or transesophageal) is non-(or minimally) invasive, can be performed at the bedside, and is relatively inexpensive. While 2D echocardiography provides higher temporal resolution (30–100 fps), current 3D volumetric ultrasound sequences are limited to about 20 volumes per second although newer methods to increase this frame rate are being devised [42]. The high temporal resolution of Echo allows for single-beat reconstruction of heart motion which is essential when modeling hemodynamics in arrhythmic hearts. Echo can even enable tracking of the valve leaflets which can help in parameterizing valve models. However, from the viewpoint of CFD model construction, the primary disadvantage of Echo is the presence of significant noise which reduces effective resolution, and creates difficulties for a clear delineation of the chamber lumen (see Fig. 6(a)) as well as small scale features such as trabeculae and papillary muscles. However, given the wide spread availability and low cost of echocardiography, hemodynamic modeling based on echocardiography would significantly expand the reach of simulation-based therapies.

Cardiac CT (CCT) is another modality that provides very high spatial resolution to extract the ventricular lumen with reasonable temporal resolution. Current CT technology provides high isotropic spatial resolution (about 0.5 mm) and reasonable temporal resolution in the range of 50–175 ms, depending on the scanner platform and the acquisition protocol used. Acquisition times are rapid, varying from 5–10 seconds for 64 detector systems to as little as 275 ms for 320 detector systems, and CT images can be acquired with effective radiation doses often less than background radiation from environmental sources [43]. Several systems are now capable of whole heart isotemporal acquisitions over portions of a single heartbeat [44–46]. The quality of the CT image and the enhanced lumen delineation via the use of intravenous contrast agents make CT ideal for 4D endocardial surface extraction for subsequent computational modeling (see Fig. 6(b)). Although the level of radiation exposure and the associated hazards are still debatable [47–49], this technology has a promising future with the development of fifth generation designs incorporating advanced technologies such as wide area detectors, myocardial perfusion imaging, dual energy and spectral imaging technologies [50–52].

Cardiac MR is non-invasive, it does not pose a radiation hazard and it provides 4D images of heart. Phase-contrast MR mapping can also provide intracardiac velocity fields. However, while CMR has a high in-plane resolution (1.5 mm), the through-plane resolution is much lower (typically about 8 mm, see Fig. 6(c)). This, and through-plane motion poses a challenge for accurate segmentation of the cardiac lumen. Furthermore, the large acquisition times makes MR imaging subject to motion artifacts and CMR imaging protocols typically rely on multi-beat acquisition and phase-averaging. This eliminates the possibility of MR based hemodynamic modeling and analysis for conditions such as cardiac arrhythmia where cardiac motion can be highly non-periodic.

#### 4.2. CFD-ready model generation

In order to generate a patient-specific, 4D, CFD-ready model from any imaging modality, a set of images covering one or more cardiac cycles need to be segmented and concatenated. The segmentation of images and generation of a 3D model can be done using available software tools such as Mimics™ [53], MIPAV (NIH) [54], ITK-SNAP [55], Seg-3D [56], TurtleSeg ([www.turtleseg.org](http://www.turtleseg.org)) [57,58], 3D-Doctor [59], MITK [60] and GIMIAS [61], many of which are open-source tools.

The degree of human intervention required in the image segmentation step depends on a number of factors such as image quality and resolution, but in virtually no case, can this process be fully automated. In fact, our current experience in developing CFD-ready models of the left-ventricle indicates that a minimum of 20 key time frames per cardiac cycle need to be segmented and reconstructed. Although one can obtain a set of time dependent 3D models of heart by the segmentation, these models cannot usually be used directly for the hemodynamic simulation. This is because the time dependent 3D models should have a consistent topology and surface mesh properties (e.g. connectivity) to generate kinematic boundary condition on the moving endocardial surface, and most of the segmentation/model construction tools do not guarantee such consistency. Generation of one CFD-ready model from images therefore currently requires significant human effort (anywhere from 20–50 hours of work) and remains the largest bottleneck in these simulations. Thus, there is a clear need to create an efficient and automated pipeline for generating CFD-ready models from cardiac imaging and a number of groups are working on this using a variety of methods [62–70]. A promising new approach is that of [71] where the modeling of flow in biological configurations is based on level sets derived directly from images and eliminates the intermediate step of surface mesh generation. However, this method is currently limited to relatively simple geometries and motions.

In our research we are employing template based geometric model construction techniques. In this approach, to generate patient-specific LV model, we map a template LV surface to the patient-specific target at each key frame, which is a surface obtained from the segmentation of CT, MR, or, Echo images. The mapping can in-principle be accomplished by a variety of surface matching algorithms [62,72–77] but methods such as Iterative Closest Point (ICP) [78] and elastic deformation algorithms [79,80] are not diffeomorphic and are only suitable for small local deformations. The cardiac lumen surfaces of interest here undergo large deformations, and here we employ a diffeomorphic registration algorithm known as Large Deformation Diffeomorphic Metric Mapping (LDDMM) [81,82]. In the LDDMM framework, the surfaces and curves are viewed as manifolds embedded in three-dimensional space, and the deformation is a diffeomorphism  $\phi$ . In other words, the mapping  $\phi$  is a smooth onto mapping with a smooth inverse. Therefore, it preserves the topology of the surfaces and avoids creating singularities or self-intersections of the computing grid even for large deformations. The diffeomorphisms are generated via flows of the differential equation

$$\partial_t \phi(x, t) = v(\phi(x, t), t); \quad \phi(x, 0) = x. \quad (1)$$

The vector velocity field  $v$  belongs to a reproducing kernel Hilbert space (RKHS) [83]. The registration algorithm minimizes the cost function which consists of the norm of  $v$ , which controls the smoothness of the deformation, and the disparity between the mapped template and the target. The algorithm used to minimize this cost function is described in detail in [84]. For a triangulated surface template with nodes, the topology of the triangulated surface remains unchanged, and only the nodes are moved with the optimal velocity,  $v$  which minimize the cost function.

The disparity or mismatch between the two surfaces is calculated via a mathematical formulation in which the triangulated surfaces are embedded in a RKHS. The RKHS norm is then used to measure the disparity [85]. The disparity between a surface and a set of cross sectional curves is defined as the sum of Euclidean distances from each point on the curve to

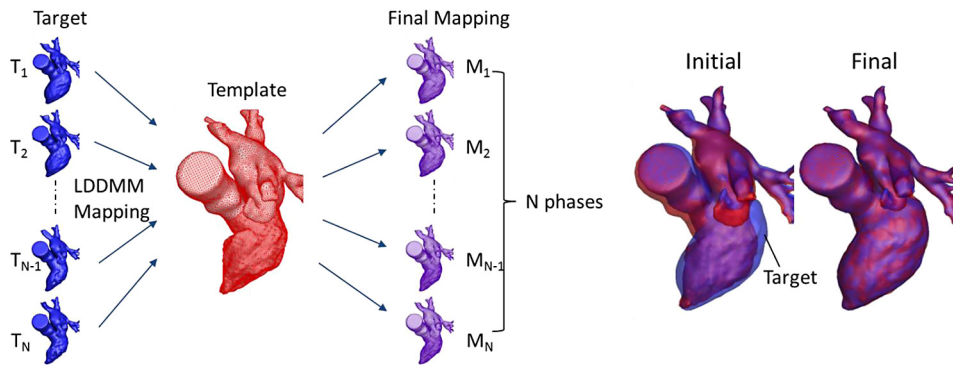


**Fig. 7.** LDDMM mapping of ‘template’ to each ‘target’ corresponding to a cardiac phase. The final smooth mapping is superposed on the corresponding target over the entire cardiac cycle. Here, the template is chosen to be the end-systolic state. (For interpretation of the references to color in this figure, the reader is referred to the web version of this article.)

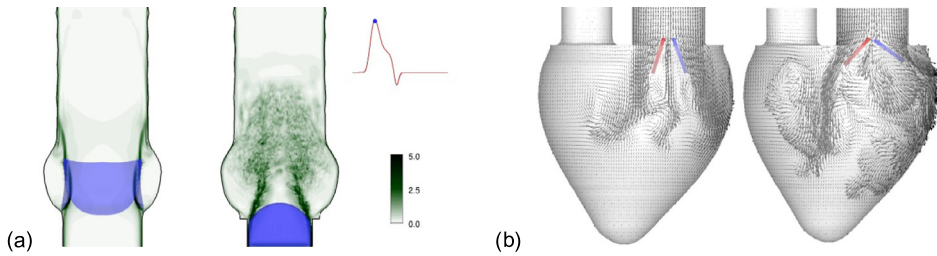
the nearest point on the surface. Details of this formulation can be found in [86]. It is pointed out that while this method appears similar to ICP, its combination with LDDMM guarantees that the deformation is a diffeomorphism.

Fig. 7 shows the LDDMM mapping of the triangulated endocardial surface of a human left-heart. The triangulation is performed subsequent to the segmentation of the CT data to extract left atrium, left ventricle and aorta. We have used a “region growing” algorithm in the commercial software Mimics® [53] to carry out this pre-processing step following which, the FEA module is used to triangulate the extracted lumen volume. Since the CT data comprises 20 cardiac phases, 20 triangulated surfaces are created for each cardiac cycle. The precursor to LDDMM mapping is to create a template as the starting point of the projection which, in the present case, is the end-systolic state as shown in Fig. 7. It is to be noted that there is no specific criterion for choosing a template. However, the convergence of LDDMM is significantly accelerated by choosing a template that is similar to the ‘target’. The template is then mapped onto each target surface corresponding to a distinct cardiac phase (blue surfaces in Fig. 7) using LDDMM. The end-result for each mapping is shown in Fig. 7 and it is evident that there is a reasonable agreement between the LDDMM mapping and the corresponding targets as shown in Fig. 7. In order to obtain the intermediate cardiac phases, we perform a smooth cubic spline interpolation of each surface coordinate in time which ensures continuity of both first and second derivatives. This is reasonable as the LDDMM mapping preserves the topology before and after the projection. One can notice that the surfaces in the present case are reasonably smooth so that one can perform the LDDMM mapping simultaneously, i.e., use a single template for all the cardiac phases. However, if the surface has complex structures such as trabeculae, or if the template is topologically highly dissimilar to the target, then it is advisable to perform LDDMM in a sequential manner wherein the output of first LDDMM mapping is used as template for the subsequent mapping and so on.

#### 4.3. Models for atrioventricular valves

The presence of the atrioventricular valves (mitral and tricuspid valves) creates a significant complication for modeling of cardiac flows since these valves are expected to have a significant effect on the ventricular flow patterns. For instance, our recent study [87] has shown that the presence of the mitral valve (MV) significantly affects the flow and its propagation into the left ventricle. Additionally, the asymmetry of the mitral valve leaflets direct the flow to impinge on the posterior wall [87] and promotes a circulatory pattern in the bulk of the ventricular cavity. Thus, inclusion of a relatively accurate model of the mitral valve seems necessary for reproducing many of the key features of the intraventricular flow field. Two basic approaches are available for modeling the mitral valve; the first is a biomechanics based approach where the valve is modeled as a deformable structure and its motion computed by modeling the fluid–structure interaction (FSI) problem. A number of groups are developing and exploring such biomechanical valve models [88–90]. The mitral valve is, however, an extremely complex structure and such models would significantly add to the overall computational effort. In addition, the less-than-complete understanding of the constitutive and structural properties of this complex structure would also add uncertainties in the simulation results. Finally, we are still far from being able to deploy *patient-specific* MV biomechanical valve models, which might be needed for many clinical applications. FSI models have however found significant use in the studies of aortic valves (both natural and prosthetic) and prosthetic mitral valves. The structure and kinematics of mechanical prosthetic valves is relatively simple and readily amenable to FSI modeling. Fig. 8(a) shows results from a FSI simulation of natural and prosthetic aortic valves [91,92] and Fig. 8(b) shows results for a bileaflet mechanical valve in the mitral position [93]. Le and Sotiropoulos performed a FSI simulation of prosthetic aortic valve in the realistic aorta coupled with LV hemodynamics [94]. The recent work of Hsu et al. [95] on the FEM FSI analysis of bio-prosthetic valve is also notable. The current efforts on the patient-specific simulation of cardiac valves by various research groups are summarized in two recent review articles [96] and [97].

The other option for the inclusion of natural mitral valves in simulations is to use a kinematic model of the valve where the geometry and movement of the leaflets is prescribed based on some measurements. For instance, all the three imaging



**Fig. 8.** (a) Comparison of total stress exerted on the blood cells for through a natural (left) and bileaflet mechanical (right) aortic valve obtained by FSI modeling [91,92] (image provided by Dr. Roberto Verzicco). Simulation indicates that the mechanical valve exposes a larger proportion of the blood cells to high stresses. (b) FSI simulation of flow and leaflet motion for a bileaflet prosthetic mitral valve. Plots show flow vectors and leaflet configuration at end-diastole for two different leaflet hinge locations [93].

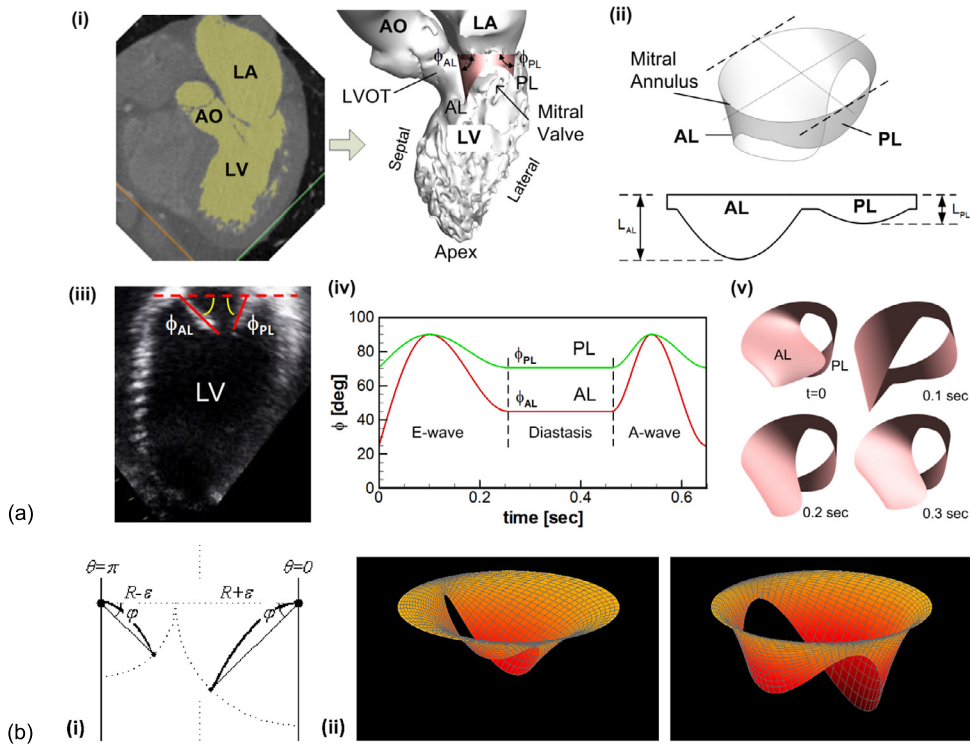


**Fig. 9.** (a) Procedure for developing a patient-specific kinematic model of the mitral valve: (i) contrast CT scan data of the normal human heart with the left heart highlighted and LV model reconstructed from this data, LA: left atrium, AO: aorta, LVOT: LV outflow tract, AL: anterior leaflet, PL: posterior leaflet,  $\phi_{AL}$ ,  $\phi_{PL}$ : AL, PL opening angles; (ii) mitral valve geometry, top: 3D shape, bottom: “unrolled” valve geometry,  $L_{AL}$ ,  $L_{PL}$ : AL, PL lengths; (iii) measurements of mitral valve leaflet opening angles with respect to the mitral annulus plane using the echocardiogram data; and (iv) time profiles of mitral valve opening angles based on in-vivo measurements; (v) MV leaflet configurations at selected phases of the cardiac cycle. (b) A reduced degree-of-freedom dynamic model of the mitral valve: (i) schematic of the model; (ii) shapes of the mitral valve model at two different phases. (Images provided by Dr. Gianni Pedrizzetti.)

modalities (Echo, CMR and CTA) can provide information about the location of the tip of the valve leaflets and this can be used to create a kinematic model of the leaflets. This latter approach is obviously not of use in situations where the interest is in predicting the motion of the leaflet such as in leaflet plication or mitral clip surgery. However, in many clinical applications such as LV thrombosis, the interest is in diastolic/systolic flow patterns in the ventricle, and in such applications, a kinematic model of the mitral valve based on patient-specific measurements would be a viable approach. Fig. 9(a) shows the key features of such a kinematic model that has been used in a fundamental study of the effect of mitral valve on diastolic flow patterns [93]. In this model, the prescribed opening angles of mitral valve leaflets are measured from the Echo data. Alternatively, Domenichini and Pedrizzetti [98] proposed a reduced degree-of-freedom model of the mitral valve (Fig. 9(b)), in which the opening angle is determined dynamically by matching to an interface condition. This dynamic model could represent the fluid–leaflet interaction naturally. The results from ventricular flow simulations that employ the kinematic MV model are presented in Figs. 11 and 12 of this article.

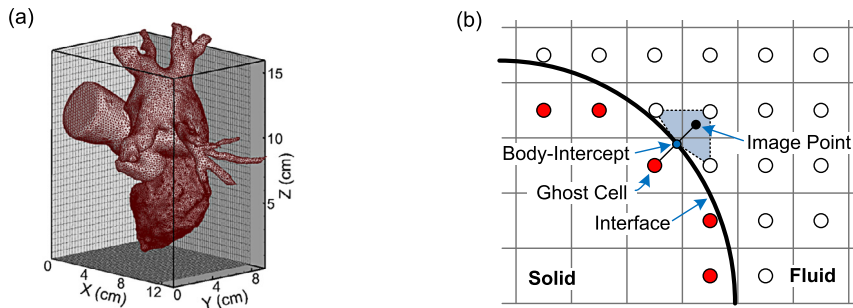


**Fig. 10.** (a) A two-chamber heart model immersed in a Cartesian volume grid. The model includes the left-atrium (LA), the left-ventricle (LV), pulmonary veins and a portion of the ascending aorta. (b) Schematic of ghost cell method for the immersed boundary treatment. The boundary condition on the body-intercept point is satisfied by imposing the value on the ghost cell. The ghost cell value is obtained from the image point which is computed by the interpolation from the surrounding fluid cells.

## 5. Cardiac flow modeling methodologies

Once the 4D kinematic model of the heart including appropriate representations of the atrioventricular valves is ready, the intracardiac blood flow is obtained by performing a computational fluid dynamic (CFD) simulation. The conventional approach to CFD modeling of flow in complex geometries employs finite-volume [21,68,99–101] or finite-element method (FEM) [7–10,102–104] with unstructured, body-conformal grids and these methods have been successfully applied to vascular flow simulations. However, given the significant wall motion and deformation associated with ventricular flows, any body-conformal grid method has to employ automatic remeshing strategies, which can significantly increase the complexity and cost of the simulation. An example of such an approach can be found in Ref. [105]. The other popular method in the simulation of cardiac flows is the immersed boundary method (IBM) [106]. In this method, the flow is resolved on a static body non-conformal grid, and the boundary condition is imposed by a localized body force or modification in the discretization procedure and this has emerged as the method of choice for cardiac simulations [15,26–29,58,59,80,83–88]. Since the volume grid for the flow simulation does not need to be deformed or remeshed to conform to the moving/deforming ventricular lumen, the IBM approach is very appropriate for the fully automated simulation of cardiac flows. Given the popularity of this method for cardiac simulations, we briefly introduce the IBM approach as applied by our group.

### 5.1. Immersed boundary flow solver

For the hemodynamic flow simulation, the surface body model of a 4D kinematic heart is immersed into the non-body conformal Cartesian volume grid (see Fig. 10(a)), and the flow simulation is performed by solving the incompressible Navier–Stokes equation using the immersed boundary method (IBM) [107]. For the cardiac blood flows, blood can be assumed as Newtonian fluid and thus its motion is governed by the incompressible Navier–Stokes equations that are written as

$$\nabla \cdot \vec{U} = 0, \quad \frac{\partial \vec{U}}{\partial t} + (\vec{U} \cdot \nabla) \vec{U} + \frac{1}{\rho_0} \nabla P = \nu_0 \nabla^2 \vec{U}, \quad (2)$$

where  $\vec{U}$  is a velocity vector,  $P$  is a pressure,  $\rho_0$  and  $\nu_0$  are the density and kinematic viscosity of the blood. While there are a number of groups that have employed different variants of the immersed boundary method to model cardiac flows [15,26–29,58,59,80,83–88] we describe the solver and the particular approach that is used by our group.

Equation (2) is solved by a projection method based approach [108]. The momentum equation is discretized by a second-order Crank–Nicolson method and the pressure Poisson equation is solved by either a geometric multi-grid method or a conjugate gradient method [109]. All the spatial derivatives are discretized by a second-order central differencing. The discretized equations are solved on the non-body conformal Cartesian grid and the complex, moving boundaries are treated by a sharp-interface immersed boundary method as described in [107]. The velocity boundary conditions on the endocardial surface are given by the 4D kinematic heart model constructed by the method described in the previous section. These boundary conditions on the endocardial surface are imposed by a multi-dimensional ghost cell method [107] as shown in Fig. 10(b). The boundary condition on the body-intercept point is satisfied by imposing the value on the ghost cell and the ghost cell value is obtained from the image point which is computed by the interpolation of values on the surrounding fluid cells. Further details regarding this method can be found in Refs. [81] and [82].

### 5.2. Hemodynamic simulation

To obtain reliable data and a detailed description of the flow, the flow simulation needs to be conducted on a grid with sufficient resolution. In this section an example of high-resolution cardiac flow simulation is presented. The simulation is carried out using the heart model shown in Fig. 7, and the surface body of the model is discretized with about 53,000

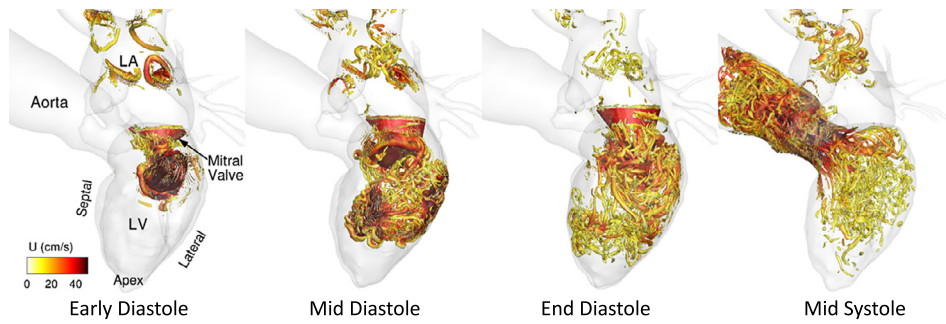


**Fig. 11.** Time evolution of intraventricular vortex structures during the whole cardiac cycle for the model shown in Fig. 6. Vortex structures are visualized using the  $\lambda_{ci}$ -criterion [110,111] and colored by the magnitude of velocity.

triangular elements. For the flow simulation, the model is immersed into the Cartesian volume of  $11.4 \text{ cm} \times 9.5 \text{ cm} \times 15.8 \text{ cm}$  and this volume is discretized into  $384 \times 256 \times 256$  cells. The total number of cells is over 25 million and the smallest dimension of each computational cell is about 0.3 mm that is finer than the resolution of the most advanced multi-detector CT scanner ( $\sim 0.5 \text{ mm}$ ). Currently the computation cost of one cardiac cycle is about 80 hours with 512 CPUs on the XSEDE (Extreme Science and Engineering Discovery Environment)'s TACC Stampede supercomputing cluster which consists of 6400 computing nodes with two Xeon E5-2680 processors with 16 cores per node and configured with 32GB memory per node. Additionally, each compute node is also configured with an Intel Phi SE10P coprocessor with an additional 8GB memory and 61 cores on the coprocessor card.

The simulated intraventricular blood flow pattern for the human left-heart is shown in Fig. 11. The end-diastolic (EDV) and end-systolic volumes (ESV) for the present model are 218 ml and 125 ml, respectively. Thus, the stroke volume and the corresponding ejection fraction can be evaluated to be 93 ml and 43%, respectively. The time evolution of three-dimensional (3D) vortical structures is shown in Fig. 11 at the indicated cardiac phases during the entire cardiac cycle. The 3D vortex structures are visualized using  $\lambda_{ci}$ -criterion defined as the complex imaginary eigen-values of the velocity gradient tensor [110,111] and are colored using the magnitude of velocity. The complex flow structure due to interaction of vortex rings ejected from the pulmonary veins into the left atrium can be noticed. Also evident from Fig. 11 is the formation of a vortex ring in the left ventricle and its subsequent wall interaction giving rise to a complex transitional flow.

Here we show results of a computational study that employs a kinematic mitral valve model where the geometry and leaflet kinematics are prescribed based on physiological measurements [87,112] of normal mitral valves. Since mitral valve undergoes large deformations which change its orifice area, position and orientation with time, we have used LDDMM to register the mitral valve model in a way similar to that of the left-heart model discussed in section 4.2. Fig. 11 shows the vortex structures for a two-chamber model of the left heart that includes left atrium and ventricles as well as the outflow tract and pulmonary veins. This model is based on dynamic CT imaging as described in 4.2 and it employs a kinematic model of the mitral valves. Figure shows the generation of vortices in the atrium as well as the ventricle during diastole and the subsequent ejection of ventricular vortices into the outflow tract during systole. Another example of a kinematic mitral valve appears in the next section.

### 5.3. Multiphysics cardiac simulations and virtual cardiography

High-fidelity cardiac flow simulations can be coupled with the simulation of other physics to further investigate the role of hemodynamics on disease progression as well as the consequences of pathological blood flow patterns. For example, a coupled hemodynamics and coagulation biochemistry simulation can be used to investigate the formation of left ventricular thrombus (LVT) in infarcted ventricles [29]. Thrombus formation is the result of a complex biochemical process that involves both the infarcted myocardium and the blood flow [113]. Since the transportation and accumulation of the biochemical species are driven by the blood flow, LV flow patterns play an important role on the LVT formation. This flow-mediated thrombus generation can be modeled by coupling the hemodynamic equations to the set of biochemical convection-diffusion-reaction (CDR) equations:

$$\frac{\partial C_i}{\partial t} + (\vec{U} \cdot \nabla) C_i = D \nabla^2 C_i + R_i, \quad (3)$$

where  $C_i$  is the concentration of  $i$ -th species,  $D$  is the diffusion coefficient, and  $R_i$  is the reaction source term which is determined by the reaction equation.

In our recent study [114], we performed the simulation of LVT formation in the canonical model of infarcted LVs by solving the incompressible Navier-Stokes equation and a total of 21 coupled CDR equations describing the coagulation cascade [115], the conversion of fibrinogen into fibrin [116], platelet activation and aggregation [117]. Fig. 12 shows recent (unpublished) simulations that predict the accumulation of coagulation factors in a modeled infarcted ventricle. These simulation results are being used to study the mechanism of flow mediated thrombogenesis, with potential use in the development

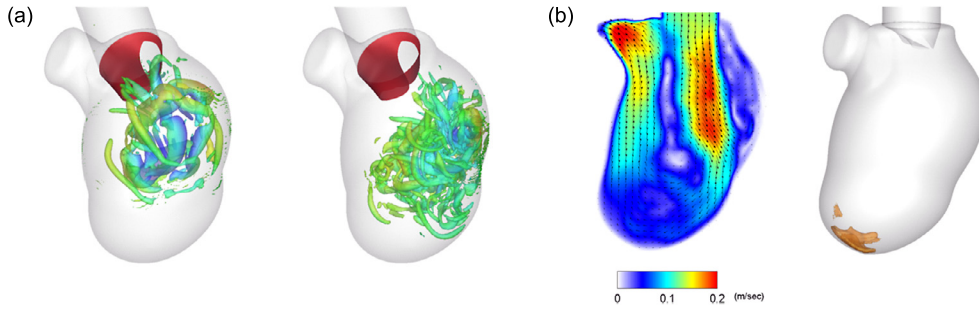


**Fig. 12.** Simulation of LVT formation in the infarcted LV with apical aneurysm. (a) Evolution of 3D vortical structure. This simulation also employs a kinematic model of the mitral valve; (b) Averaged velocity magnitude (left) showing the penetration of the mitral jet into the LV cavity and isosurface of fibrin concentration (right) used as an indicator of the thrombus.

of improved diagnostic methods for LVT. Ongoing studies are focused on validation of this method against patient-specific cases.

Abnormal blood flow pattern in the cardiovascular system generates distinct sounds which can be used for the non-invasive diagnosis of heart conditions. The development of this cardiac auscultation is, however, currently limited due to the limited-understanding of the physical mechanisms that are associated with the generation and propagation of heart sounds. By coupling cardiac flow simulations with models of acoustics, the generation and propagation of heart sounds can be simulated from first principles. A direct simulation of these processes allows us to investigate the mechanisms of heart murmurs and the characteristics of sound propagation in the thorax. We simulate the generation and propagation of blood flow-induced sounds using a hybrid approach that employs the incompressible Navier–Stokes and the linearized perturbed compressible equations (LPCE) [118,119]. In this approach, the flow-induced sound source term is obtained from the computational hemodynamic simulation and the sound propagation through the thorax is modeled with a unified set of acoustic wave equations:

$$\begin{aligned} \frac{\partial \vec{u}'}{\partial t} + H(\vec{x}) \nabla(\vec{u} \cdot \vec{U}) + \frac{1}{\rho(\vec{x})} \nabla p' &= 0, \\ \frac{\partial p'}{\partial t} + H(\vec{x}) \left[ (\vec{U} \cdot \nabla) p' + (\vec{u}' \cdot \nabla) P \right] + K(\vec{x}) (\nabla \cdot \vec{u}') &= -\frac{DP}{Dt} H(\vec{x}), \end{aligned} \quad (4)$$

where  $(')$  represents the compressible (acoustic) perturbation,  $H$  is a Heaviside function which has a value of 1 in the blood flow region and 0 elsewhere, and the density ( $\rho$ ) and bulk modulus ( $K = \rho c^2$ ) are functions of space. The capital letters  $(U, P)$  indicate the hydrodynamic incompressible flow variables and they are obtained from the incompressible flow simulations. The details of this procedure can be found in [23] and Fig. 13 shows some representative results from a heart sound simulation. This computational “hemoacoustic” simulation capability can be used to generate insights into the correlation between disease and murmur and has the potential to improve the diagnostic ability of cardiac auscultation.

The flow field data obtained from the simulation can be post-processed to extract quantitative metrics such as the work done on the fluid flow, shear stresses, and energy dissipation. The flow data can also be used to conduct ‘virtual’ cardiography. For example, a Doppler ultrasound image which depicts intraventricular flow motions can be reproduced by the post-processing of the flow field result. This is done by the Lagrangian particle tracking of virtual red blood cell (RBC) and applying sound wave scattering theory [120]. The motion of RBC particles is tracked by using the time-dependent Eulerian velocity field obtained from the cardiac flow simulation and ultrasound wave propagation and scattering by RBC particles are described by an acoustic analogy for arbitrary ultrasound transducer/receiver shape. The ultrasound wave signal scattered by each RBC particle can be expressed as

$$s_n(t) = \frac{R}{(2\pi)^2} \int_{S_2} \int_{S_1} \frac{1}{r_2(\mu)} \frac{1}{r_1(\mu)} e^{i(\mu - r_1(\mu)/c)} dS_1 dS_2, \quad (5)$$

where  $S_1$  and  $S_2$  represent transducer and receiver surfaces,  $r_1$  and  $r_2$  are distances from the RBC particle to the point on the transducer and receiver surfaces, respectively,  $R$  is a constant reflection coefficient,  $e$  is the time function of emitted signal on the transducer,  $\mu$  is the retarded time, and  $c$  is the speed of sound. The total scattered signal is obtained by the summation  $s_n(t)$  for all the RBC particles.

Once the time series of scattered ultrasound signal is obtained on the receiver, a Doppler ultrasound image can be constructed by a signal processing such as a time-frequency spectrogram. Further details of the procedure can be found in Ref. [23]. Fig. 14 shows the examples of virtual Doppler diagrams; virtual pulsed wave Doppler diagram for the mitral inflow made by using the simulated flow field result. The present ultrasound simulation method allows us to reproduce echo Doppler diagrams that are inline with those measured at the clinical bedside (see Fig. 14(b) and (c)). Thus, as mentioned

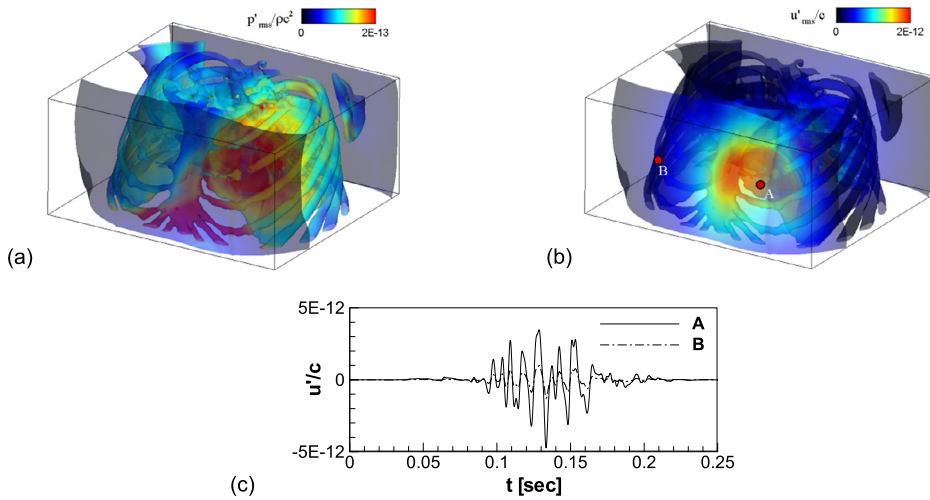


**Fig. 13.** Example of computational hemoacoustic simulation for a systolic HOCM murmur radiated in a realistic human thorax model based on the Visible Human<sup>®</sup> <sup>1</sup> Dataset. (a), (b): Root-mean-squared acoustic pressure and velocity fluctuations plotted on the density iso-surfaces. (c): Phonocardiographic signals for the HOCM systolic murmur show measurable differences in the monitored acoustic signal at points A and B on the precordium in figure (b). The signals are band-pass filtered for the range 20–400 Hz. In these figures,  $\rho$  and  $c$  are the density of blood and the speed of sound in the body.

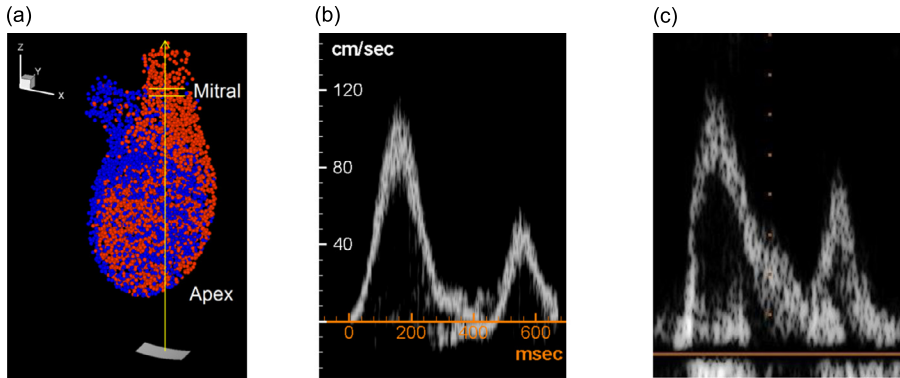


**Fig. 14.** Examples of virtual Doppler cardiograms made with cardiac flow simulation results. (a) RBC particles and ultrasound transducer/receiver surface. The location of sample volume is also indicated. (b) Virtual pulsed wave Doppler for the mitral inflow based on CFD data. Positive values indicate velocity toward the apex. (c) Pulsed wave Doppler for the mitral inflow measured for a patient. Note that the patient condition is different from the simulation shown in Fig. 14(a) and (b).

earlier, these virtual echo-cardiographic plots can be directly and easily compared to the clinically measured ones to verify the fidelity of patient-specific cardiac flow simulations.

### 6. Simulation acceleration by GPUs

Significant reductions in turn-around time of cardiac flow simulations are essential for successful clinical translation of simulation-based diagnosis and treatment of cardiac disease. One effective way to achieve such a speed-up is through the utilization of advanced graphical processing units (GPUs). In general, since GPUs have large processing cores counts (512 and higher) per unit and also have the ability to perform rapid floating point operations, they are ideal for the speeding-up of large scale scientific computations such as flow simulations. Furthermore, the development of GPUs is driven mostly by popular applications such as gaming and video rendering and these provide a powerful incentive for continuous performance improvement and cost reduction of this technology. However, the successful speed-up of large scale computations using GPUs depends on the data parallelism, available memory size, data transfer between CPU and GPU, and the associated code optimization. Especially for the large scale CFD problems such as cardiac flow simulations that cannot be handled by a couple of GPUs, the optimization of data transfer between multiple GPUs on the multiple machines is the key to the acceleration. The biggest hurdles in this data transfer optimization on GPUs are primarily due to small on-chip memory,

<sup>1</sup> Anatomical data set developed under contract from the National Library of Medicine by the Departments of Cellular and Structural Biology, and Radiology, University of Colorado School of Medicine.

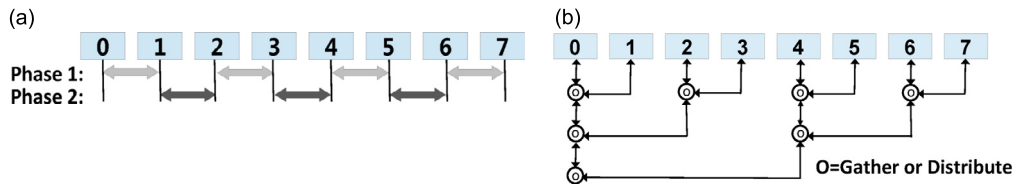


Fig. 15. (a) Two phase vector communication technique with neighboring machines. (b) Tree topology based scalar broadcasting/gathering technique.

large communication times and load-imbalance. In this section, we briefly describe our efforts to address this issue in accelerating cardiac flow simulations using GPUs.

The most time consuming part in the hemodynamic flow simulation is the solution of the coupled linear system of equations that result from the discretization of the governing equations (Eq. (2)). To achieve a significant speed-up of our flow solver by utilizing advanced GPU computation technique, we have ported the solution procedure of the linear system of equations from CPUs to GPUs. We have recently developed a GPU-based BiCGSTAB solver (GBCG) [121] that meets both generalizability and scalability requirements. It is well suited for all types of banded linear systems and this solver combines a new matrix decomposition method with several optimizations for inter-GPU and inter-machine communications to achieve good scalability on large-scale GPU clusters. Our approach of matrix decomposition is to factorize the large matrix into smaller sub-matrices in the row-oriented fashion, and solve the sub-linear systems in parallel. For a generic linear system like the Poisson and advection diffusion equations that are generated from the solution procedure of the Navier–Stokes equations, large matrices cannot be partitioned into independent sub-matrices, and communication is therefore required. Since the construction of the matrix is already done row-wise in the target problem, our method requires no additional communication during matrix decomposition, for every machine solves the rows it has already constructed. However, a number of data transfers are still required in the solution procedure. For example, the correlation of the sub-matrices is maintained by a vector communication before the Sparse Matrix-Vector Multiplication (SpMV). Specifically, each machine communicates with its neighboring machines to update the vectors that are needed by the boundary rows of the sub-matrices during SpMV operations.

Our vector communication leverages three optimization techniques. First, we utilize registered memory for MPI data exchange. Specifically, the send and receive buffers are allocated as pinned memory, and we use the pinned flag to communicate the virtual-to-physical address mapping of the sending and receiving buffers to the network adapter. Second, we overlap the copying of sending data from GPU to CPU with GPU computation. Third, we exploit two-phase communication strategy to overcome communication congestion. Fig. 15(a) presents the two-phase strategy with eight machines. In the first phase, we allow machine pairs [0 1], [2 3], ..., [6 7] to communicate. In the second phase, the [1 2], [3 4], ..., [5 6] machine pairs talk with each other. Compared to native implementation, two-phase optimization alone renders 3x speedup, and the combination of two-phase and registered memory optimizations enables our solver to achieve 70% of idealized communication bandwidth [121].

For the optimized scalar communication, we apply a tree-based broadcast method for all the participating machines. Specifically, our solver conducts scalar communication for exchanging the global maximum or global sum information across all the machines. In the native implementation, every machine simply conducts the broadcast and performs the calculation. This introduces both network congestion and long communication time. Fig. 15(b) describes our tree topology based broadcast method. The scalar variable from each machine is gathered to one machine in a tree based manner. Afterwards, the result is distributed to all machines in the reverse order. Through this optimization, the number of scalar communication decreases significantly. Our test cases show that the scalar communication time is reduced by about 1/64 [121].

The performance of GPU implementation of our flow solver with optimized communication techniques has been tested for the cardiac flow simulation on the GPU-cluster (NICS-Keeneland: Each node is equipped with two 8-core Xeon E5 processors, three NVIDIA M-class GPUs codenamed Fermi M2090 which has 512 CUDA cores and 6GB GDDR5 memory, and the main memory (DRAM) size of each node is 32GB) with up to 192 GPUs. Fig. 16 shows the scalability trends for the increasing problem sizes (small:  $128^3$ , medium:  $256^3$ , large:  $256^2 \times 512$ ). As expected, the GPU-based conjugate gradient solver (GBCG) does not scale well for the small problem size on 192 GPUs, since the ratio of communication to the computation time is found to be 61.2%. For the medium size problem however, this ratio reduces to 32.1% and it further decreases to 18.3% for the large size problem. The decrease of communication-to-computation ratio is associated with an increased parallel computing efficiency and both the medium and large problems scale well on up to O(100) GPUs with computational speeds reaching up to about 4 TFLOPS on 192 GPUs. It is noted that (see Fig. 3) this performance is nearly sufficient to be deployed for the simulations of cardiac conditions where the planning stage for surgeries extends over many days or weeks such as valve repair or implantation, HOCM and CRT, to name a few.

## 7. Concluding remarks

In the article we have summarized the current status and future outlook for modeling and simulation of cardiac hemodynamics i.e., the blood flow in the chambers (atria and ventricles) of the heart. A case is made that modeling and simulation of cardiac flows enabled by computing capabilities that are becoming increasingly powerful and cost effective over time,

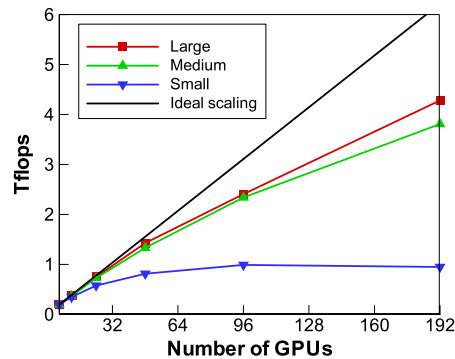


Fig. 16. Parallel scaling of the cardiac flow solver on a GPU machine for three different problem sizes; small:  $128^3$ , medium:  $256^3$ , large:  $256^2 \times 512$ .

provide an effective means for counterbalancing the adverse trends in incidence as well as expenditure associated with cardiovascular disease. Computational modeling of cardiac flows could be deployed to enhance existing diagnostic procedures as well as to assess options in treatment and cardiac surgery. In terms of the former, computational modeling could, for instance, improve stratification of risk for left-ventricular thrombogenesis in infarcted ventricles, and a comprehensive analysis of the physics of heart murmurs enabled by computational models could lead to more effective automated cardiac auscultation techniques. For the latter, near term opportunities exist in surgical planning for myocardial resection in obstructive HOCM, leaflet plication in SAM, valve repair and prosthetic valve implantation as well as patient-specific optimization of LVADs. However, cardiac flows present features such as large-scale motion and deformation, fluid–structure interaction of the valves, and a relatively high Reynolds number, all of which significantly increase the challenge for computational modeling and simulation. These challenges include: (a) large computational times requiring computational speeds exceeding  $O(10)$  TFLOPS for clinical application; (b) need for rapid and effective methods for converting clinical images to computation-ready models; (c) appropriate models of atrio-ventricular valves; and (d) methods for rapid validation of patient-specific computational models. Finally, in order to reach its full potential in clinical applications, computational models of cardiac flows will have to incorporate additional physics such as structural dynamics, acoustics, electromechanics and biochemistry, and will also have to exploit emerging trends in computing such as GPU based acceleration and commodity computing.

## Acknowledgements

R.M. acknowledges support from National Science Foundation through grants IOS-1124804 and IIS-1344772 as well as Extreme Science and Engineering Discovery Environment (XSEDE) through NSF grant number TG-CTS100002. R.M. and R.T.G. also acknowledge support from the Discovery Fund Synergy Award from Johns Hopkins University. The development of the IB flow solver described here benefited from support from AFOSR, NASA, and NIH. The authors wish to express gratitude to Drs. David Nordsletten, Roberto Verzicco, and Gianni Pedrizzetti for kindly providing images from their research.

## References

- [1] D. Mozaffarian, E.J. Benjamin, A.S. Go, D.K. Arnett, M.J. Blaha, M. Cushman, S. de Ferranti, J.P. Despres, H.J. Fullerton, V.J. Howard, et al., Heart disease and stroke statistics – 2015 update: a report from the American heart association, *Circulation* 131 (4) (2015) e29.
- [2] M. Fox, S. Mealing, R. Anderson, J. Dean, K. Stein, A. Price, R. Taylor, The clinical effectiveness and cost-effectiveness of cardiac resynchronisation (biventricular pacing) for heart failure: systematic review and economic model, *Health Technol. Assess.* 11 (47) (2007).
- [3] R.R. Schaller, Moore's law: past, present and future, *IEEE Spectr.* 34 (6) (1997) 52–59.
- [4] K.D. Lau, C.A. Figueroa, Simulation of short-term pressure regulation during the tilt test in a coupled 3D–0D closed-loop model of the circulation, *Biomech. Model. Mechanobiol.* (2015) 1–15.
- [5] M.E. Moghadam, I.E. Vignon-Clementel, R. Figliola, A.L. Marsden, M.O.C.H.A. (Mocha) Investigators, et al., A modular numerical method for implicit 0D/3D coupling in cardiovascular finite element simulations, *J. Comput. Phys.* 244 (2013) 63–79.
- [6] J.K. Min, J. Leipsic, M.J. Pencina, D.S. Berman, B.-K. Koo, C. van Mieghem, A. Erglis, F.Y. Lin, A.M. Dunning, P. Apruzzese, et al., Diagnostic accuracy of fractional flow reserve from anatomic CT angiography, *JAMA* 308 (12) (2012) 1237–1245.
- [7] C.A. Taylor, T.A. Fonte, J.K. Min, Computational fluid dynamics applied to cardiac computed tomography for noninvasive quantification of fractional flow reserve: scientific basis, *J. Am. Coll. Cardiol.* 61 (22) (2013) 2233–2241.
- [8] E. Kung, A. Baretta, C. Baker, G. Arbia, G. Biglino, C. Corsini, S. Schievano, I.E. Vignon-Clementel, G. Dubini, G. Pennati, et al., Predictive modeling of the virtual hemi-Fontan operation for second stage single ventricle palliation: two patient-specific cases, *J. Biomech.* 46 (2) (2013) 423–429.
- [9] C. Long, M.-C. Hsu, Y. Bazilevs, J. Feinstein, A. Marsden, Fluid–structure interaction simulations of the Fontan procedure using variable wall properties, *Int. J. Numer. Methods Biomed. Eng.* 28 (5) (2012) 513–527.
- [10] D. Sengupta, A.M. Kahn, J.C. Burns, S. Sankaran, S.C. Shadden, A.L. Marsden, Image-based modeling of hemodynamics in coronary artery aneurysms caused by Kawasaki disease, *Biomech. Model. Mechanobiol.* 11 (6) (2012) 915–932.
- [11] B. Heric, B.W. Lytle, D.P. Miller, E.R. Rosenkranz, H.M. Level, D.M. Cosgrove, Surgical management of hypertrophic obstructive cardiomyopathy: early and late results, *J. Thorac. Cardiovasc. Surg.* 110 (1) (1995) 195–208.
- [12] E.N. Feins, H. Yamauchi, G.R. Marx, F.P. Freudenthal, H. Liu, P.J. del Nido, N.V. Vasilyev, Repair of posterior mitral valve prolapse with a novel leaflet plication clip in an animal model, *J. Thorac. Cardiovasc. Surg.* 147 (2) (2014) 783–791.
- [13] K. Slocum, F.D. Pagani, K. Aaronson, et al., Heart transplantation and left ventricular assist devices, *Inpatient Cardiovasc. Med.* (2014) 197–205.

- [14] E. Deviri, P. Sareli, T. Wisenbaugh, S.L. Cronje, Obstruction of mechanical heart valve prostheses: clinical aspects and surgical management, *J. Am. Coll. Cardiol.* 17 (3) (1991) 646–650.
- [15] V. Babaliaros, A. Cribier, C. Agatiello, Surgery insight: current advances in percutaneous heart valve replacement and repair, *Nat. Clin. Pract. Cardiovasc. Med.* 3 (5) (2006) 256–264.
- [16] C. Linde, K. Ellenbogen, F.A. McAlister, Cardiac resynchronization therapy (CRT): clinical trials, guidelines, and target populations, *Heart Rhythm* 9 (8) (2012) S3–S13.
- [17] T. Doenst, K. Spiegel, M. Reik, M. Markl, J. Hennig, S. Nitzsche, F. Beyersdorf, H. Oertel, Fluid-dynamic modeling of the human left ventricle: methodology and application to surgical ventricular reconstruction, *Ann. Thorac. Surg.* 87 (4) (2009) 1187–1195.
- [18] T.B. Le, F. Sotiropoulos, On the three-dimensional vortical structure of early diastolic flow in a patient-specific left ventricle, *Eur. J. Mech. B, Fluids* 35 (2012) 20–24.
- [19] Q. Long, R. Merrifield, X. Xu, P. Kilner, D. Firmin, G. Yang, Subject-specific computational simulation of left ventricular flow based on magnetic resonance imaging, *Proc. Inst. Mech. Eng., H J. Eng. Med.* 222 (4) (2008) 475–485.
- [20] J.O. Mangual, E. Kraigher-Krainer, A. De Luca, L. Toncelli, A. Shah, S. Solomon, G. Galanti, F. Domenichini, G. Pedrizzetti, Comparative numerical study on left ventricular fluid dynamics after dilated cardiomyopathy, *J. Biomech.* 46 (10) (2013) 1611–1617.
- [21] N.R. Saber, N.B. Wood, A. Gosman, R.D. Merrifield, G.-Z. Yang, C.L. Charrier, P.D. Gatehouse, D.N. Firmin, Progress towards patient-specific computational flow modeling of the left heart via combination of magnetic resonance imaging with computational fluid dynamics, *Ann. Biomed. Eng.* 31 (1) (2003) 42–52.
- [22] J.H. Seo, R. Mittal, Effect of diastolic flow patterns on the function of the left ventricle, *Phys. Fluids* 25 (11) (2013) 110801.
- [23] J.H. Seo, V. Vedula, T. Abraham, R. Mittal, Multiphysics computational models for cardiac flow and virtual cardiography, *Int. J. Numer. Methods Biomed. Eng.* 29 (8) (2013) 850–869.
- [24] D. Tang, C. Yang, T. Geva, P.J. del Nido, Image-based patient-specific ventricle models with fluid–structure interaction for cardiac function assessment and surgical design optimization, *Progr. Pediatr. Cardiol.* 30 (1) (2010) 51–62.
- [25] X. Zheng, J. Seo, V. Vedula, T. Abraham, R. Mittal, Computational modeling and analysis of intracardiac flows in simple models of the left ventricle, *Eur. J. Mech. B, Fluids* 35 (2012) 31–39.
- [26] S. Hendabadi, J. Bermejo, Y. Benito, R. Yotti, F. Fernandez-Aviles, J.C. Del Alamo, S.C. Shadden, Topology of blood transport in the human left ventricle by novel processing of Doppler echocardiography, *Ann. Biomed. Eng.* 41 (12) (2013) 2603–2616.
- [27] M. Courtois, S. Kovacs, P. Ludbrook, Transmittal pressure-flow velocity relation. Importance of regional pressure gradients in the left ventricle during diastole, *Circulation* 78 (3) (1988) 661–671.
- [28] Y. Ishida, J. Meisner, K. Tsujioka, J. Gallo, C. Yoran, R. Frater, E. Yellin, Left ventricular filling dynamics: influence of left ventricular relaxation and left atrial pressure, *Circulation* 74 (1) (1986) 187–196.
- [29] R. Delewi, F. Zijlstra, J.J. Piek, Left ventricular thrombus formation after acute myocardial infarction, *Heart* 98 (23) (2012) 1743–1749.
- [30] N.A. Trayanova, Computational cardiology: the heart of the matter, *ISRN Cardiol.* 2012 (2012).
- [31] A. Krishnamurthy, C.T. Villongco, J. Chuang, L.R. Frank, V. Nigam, E. Belezouli, P. Stark, D.E. Krummen, S. Narayan, J.H. Omens, et al., Patient-specific models of cardiac biomechanics, *J. Comput. Phys.* 244 (2013) 4–21.
- [32] B. Baillargeon, N. Rebelo, D.D. Fox, R.L. Taylor, E. Kuhl, The living heart project: a robust and integrative simulator for human heart function, *Eur. J. Mech. A, Solids* 48 (2014) 38–47.
- [33] A. Prakosa, P. Malamas, S. Zhang, F. Pashkhanloo, H. Arevalo, D. Herzka, A. Lardo, H. Halperin, E. McVeigh, N. Trayanova, et al., Methodology for image-based reconstruction of ventricular geometry for patient-specific modeling of cardiac electrophysiology, *Prog. Biophys. Mol. Biol.* 115 (2) (2014) 226–234.
- [34] F. Vadakkumpadan, H. Arevalo, N.A. Trayanova, Patient-specific modeling of the heart: estimation of ventricular fiber orientations, *J. Visual. Exp.: JoVE* (71) (2013).
- [35] Y.J. Choi, J. Constantino, V. Vedula, N. Trayanova, R. Mittal, A new MRI-based model of heart function with coupled hemodynamics and application to normal and diseased canine left ventricles, *Front. Bioeng. Biotechnol.* 3 (2015) 140.
- [36] M. McCormick, D.A. Nordsletten, D. Kay, N. Smith, Simulating left ventricular fluid–solid mechanics through the cardiac cycle under LVAD support, *J. Comput. Phys.* 244 (2013) 80–96.
- [37] M. McCormick, D. Nordsletten, P. Lamata, N.P. Smith, Computational analysis of the importance of flow synchrony for cardiac ventricular assist devices, *Comput. Biol. Med.* 49 (2014) 83–94.
- [38] C.S. Peskin, Flow patterns around heart valves: a numerical method, *J. Comput. Phys.* 10 (1972) 252–271.
- [39] C.S. Peskin, Numerical analysis of blood flow in the heart, *J. Comput. Phys.* 25 (1977) 220–252.
- [40] C.S. Peskin, D.M. McQueen, A three-dimensional computational model of blood flow in the heart: I. Immersed elastic fibers in a viscous incompressible fluid, *J. Comput. Phys.* 81 (1989) 372–405.
- [41] D.M. McQueen, C.S. Peskin, A three-dimensional computational model of blood flow in the heart: II. Contractile fibers, *J. Comput. Phys.* 82 (1989) 289–297.
- [42] D.P. Perrin, N.V. Vasilyev, G.R. Marx, J. Pedro, Temporal enhancement of 3D echocardiography by frame reordering, *JACC: Cardiovasc. Imaging* 5 (3) (2012) 300–304.
- [43] M.Y. Chen, S.M. Shanbhag, A.E. Arai, Submillisievert median radiation dose for coronary angiography with a second-generation 320-detector row CT scanner in 107 consecutive patients, *Radiol.* 267 (1) (2013) 76–85.
- [44] K. Kitagawa, A.C. Lardo, J.A. Lima, R.T. George, Prospective ECG-gated 320 row detector computed tomography: implications for CT angiography and perfusion imaging, *Int. J. Cardiovasc. Imaging* 25 (2) (2009) 201–208.
- [45] S. Achenbach, M. Marwan, D. Ropers, T. Schepis, T. Pflederer, K. Anders, A. Kuettner, W.G. Daniel, M. Uder, M.M. Lell, Coronary computed tomography angiography with a consistent dose below 1 mSv using prospectively electrocardiogram-triggered high-pitch spiral acquisition, *Eur. Heart J.* 31 (3) (2010) 340–346.
- [46] W.H. Yin, B. Lu, Z.H. Hou, N. Li, L. Han, Y.J. Wu, H.X. Niu, J.R. Silverman, C.N. De Cecco, U.J. Schoepf, Detection of coronary artery stenosis with sub-millisievert radiation dose by prospectively ECG-triggered high-pitch spiral CT angiography and iterative reconstruction, *Eur. Radiol.* 23 (11) (2013) 2927–2933.
- [47] R. Smith-Bindman, Is computed tomography safe, *N. Engl. J. Med.* 363 (1) (2010) 1–4.
- [48] R. Smith-Bindman, D.L. Miglioretti, E. Johnson, C. Lee, H.S. Feigelson, M. Flynn, R.T. Greenlee, R.L. Kruger, M.C. Hornbrook, D. Roblin, et al., Use of diagnostic imaging studies and associated radiation exposure for patients enrolled in large integrated health care systems, 1996–2010, *J. Am. Med. Assoc.* 307 (22) (2012) 2400–2409.
- [49] C. Storrs, How much do CT scans increase the risk of cancer?, *Sci. Am.* 309 (1) (2013).
- [50] R.T. George, V.C. Mehra, M.Y. Chen, K. Kitagawa, A. Arbab-Zadeh, J.M. Miller, M.B. Matheson, A.L. Vavere, K.F. Kofoed, C.E. Rochitte, et al., Myocardial CT perfusion imaging and SPECT for the diagnosis of coronary artery disease: a head-to-head comparison from the CORE320 multicenter diagnostic performance study, *Radiol.* 272 (2) (2014) 407–416.

- [51] M. Weinger, U.J. Schoepf, A. Ramachandra, C. Fink, G.W. Rowe, P. Costello, T. Henzler, Adenosine-stress dynamic real-time myocardial perfusion CT and adenosine-stress first-pass dual-energy myocardial perfusion CT for the assessment of acute chest pain: initial results, *Eur. J. Radiol.* 81 (12) (2012) 3703–3710.
- [52] T.A. Fuchs, J. Stehli, M. Fiechter, S. Dougoud, C. Gebhard, J.R. Ghadri, L. Husmann, O. Gaemperli, P.A. Kaufmann, First experience with monochromatic coronary computed tomography angiography from a 64-slice CT scanner with Gemstone Spectral Imaging (GSI), *J. Cardiovasc. Comput. Tomogr.* 7 (1) (2013) 25–31.
- [53] Mimics, Materialise Inc., 2014.
- [54] M.J. McAuliffe, F.M. Lalonde, D. McGarry, W. Gandler, K. Csaky, B.L. Trus, Medical image processing, analysis and visualization in clinical research, in: *Proceedings of the Fourteenth IEEE Symposium on Computer-Based Medical Systems*, Washington, DC, USA, 2001.
- [55] P.A. Yushkevich, J. Piven, H.a.G.S.R. Cody Hazlett, S. Ho, J.C. Gee, G. Gerig, User-guided {3D} active contour segmentation of anatomical structures: significantly improved efficiency and reliability, *NeuroImage* 31 (3) (2006) 1116–1128.
- [56] CIBC, 2014.
- [57] A. Top, G. Hamarneh, R. Abugharbieh, Active learning for interactive 3D image segmentation, in: *Medical Image Computing and Computer-Assisted Intervention, MICCAI*, 2011.
- [58] A. Top, G. Hamarneh, R. Abugharbieh, Spotlight: automated confidence-based user guidance for increasing efficiency in interactive 3D image segmentation, in: *Medical Image Computing and Computer-Assisted Intervention Workshop on Medical Computer Vision, MICCAI MCV*, 2010.
- [59] 3D-Doctor brochure, Abel Software Corp., 2014.
- [60] I. Wolf, M. Vetter, I. Wegner, M. Nolden, T. Bottger, M. Hastenteufel, M. Schobinger, T. Kunert, H.-P. Meinzer, The medical imaging interaction toolkit (MITK): a toolkit facilitating the creation of interactive software by extending VTK and ITK, in: *Medical Imaging 2004*, 2004.
- [61] I. Larrabide, P. Omedas, Y. Martelli, X. Planes, M. Nieber, J.A. Moya, C. Butakoff, R. Sebastian, O. Camara, M. De Craene, et al., GIMIAS: an open source framework for efficient development of research tools and clinical prototypes, in: *Functional Imaging and Modeling of the Heart*, Springer, 2009, pp. 417–426.
- [62] T. McInerney, D. Terzopoulos, A dynamic finite element surface model for segmentation and tracking in multidimensional medical images with application to cardiac 4D image analysis, *Comput. Med. Imaging Graph.* 19 (1) (1995) 69–83.
- [63] D. Shen, H. Sundar, Z. Xue, Y. Fan, H. Litt, Consistent estimation of cardiac motions by 4D image registration, in: *Medical Image Computing and Computer-Assisted Intervention, MICCAI 2005*, Springer, 2005, pp. 902–910.
- [64] J.M. Peyrat, H. Delingette, M. Sermesant, X. Pennec, C. Xu, N. Ayache, Registration of 4D time-series of cardiac images with multichannel diffeomorphic demons, in: *Medical Image Computing and Computer-Assisted Intervention, MICCAI 2008*, Springer, 2008, pp. 972–979.
- [65] H. Sundar, H. Litt, D. Shen, Estimating myocardial motion by 4D image warping, *Pattern Recognit.* 42 (11) (2009) 2514–2526.
- [66] M. Gao, J. Huang, S. Zhang, Z. Qian, S. Voros, D. Metaxas, L. Axel, 4D cardiac reconstruction using high resolution CT images, in: *Functional Imaging and Modeling of the Heart*, Springer, 2011, pp. 153–160.
- [67] S. Kulp, M. Gao, S. Zhang, Z. Qian, S. Voros, D. Metaxas, L. Axel, Using high resolution cardiac CT data to model and visualize patient-specific interactions between trabeculae and blood flow, in: *Medical Image Computing and Computer-Assisted Intervention, MICCAI 2011*, Springer, 2011, pp. 468–475.
- [68] V. Mihalef, R.I. Ionasec, P. Sharma, B. Georgescu, I. Voigt, M. Suehling, D. Comaniciu, Patient-specific modelling of whole heart anatomy, dynamics and haemodynamics from four-dimensional cardiac CT images, *Interface Focus* 1 (3) (2011) 286–296.
- [69] C.W. Lim, Y. Su, S.Y. Yeo, G.M. Ng, V.T. Nguyen, L. Zhong, R. San Tan, K.K. Poh, P. Chai, Automatic 4D reconstruction of patient-specific cardiac mesh with 1-to-1 vertex correspondence from segmented contours lines, *PLoS ONE* 9 (4) (2014) e93747.
- [70] C. Chnafa, S. Mendez, F. Nicoud, Image-based large-eddy simulation in a realistic left heart, *Comput. Fluids* 94 (2014) 173–187.
- [71] S.I. Dillard, J.A. Mousef, L. Shrestha, M.L. Raghavan, S.C. Vigmstad, From medical images to flow computations without user-generated meshes, *Int. J. Numer. Methods Biomed. Eng.* 30 (10) (2014) 1057–1083.
- [72] C. Schutz, T. Jost, H. Hugli, Multi-feature matching algorithm for free-form 3D surface registration, in: *Proceedings of the Fourteenth International Conference on Pattern Recognition*, 1998, 1998.
- [73] S. Rusinkiewicz, M. Levoy, Efficient variants of the ICP algorithm, in: *Proceedings of the Third International Conference on 3-D Digital Imaging and Modeling*, 2001, 2001.
- [74] N. Litke, M. Droske, M. Rumpf, P. Schroder, An image processing approach to surface matching, in: *Symposium on Geometry Processing*, 2005.
- [75] D. Akca, Matching of 3D surfaces and their intensities, *ISPRS J. Photogramm. Remote Sens.* 62 (2) (2007) 112–121.
- [76] J. Salvi, C. Matabosch, D. Fofi, J. Forest, A review of recent range image registration methods with accuracy evaluation, *Image Vis. Comput.* 25 (5) (2007) 578–596.
- [77] J. Santamaria, O. Cordon, S. Damas, A comparative study of state-of-the-art evolutionary image registration methods for 3D modeling, *Comput. Vis. Image Underst.* 115 (9) (2011) 1340–1354.
- [78] P.J. Besl, N.D. McKay, A method for registration of 3-D shapes, *IEEE Trans. Pattern Anal. Mach. Intell.* 14 (2) (1992) 239–256.
- [79] R. Bajcsy, S. Kovacic, Multiresolution elastic matching, *Comput. Vis. Graph. Image Process.* 46 (1) (1989) 1–21.
- [80] F.L. Bookstein, Principal warps: thin-plate splines and the decomposition of deformations, *IEEE Trans. Pattern Anal. Mach. Intell.* 11 (6) (1989) 567–585.
- [81] M.I. Miller, A. Trouve, L. Younes, On the metrics and Euler–Lagrange equations of computational anatomy, *Annu. Rev. Biomed. Eng.* 4 (1) (2002) 375–405.
- [82] M.F. Beg, M.I. Miller, A. Trouve, L. Younes, Computing large deformation metric mappings via geodesic flows of diffeomorphisms, *Int. J. Comput. Vis.* 61 (2) (2005) 139–157.
- [83] N. Aronszajn, Theory of reproducing kernels, *Trans. Am. Math. Soc.* (1950) 337–404.
- [84] L. Younes, *Shapes and Diffeomorphisms*, vol. 171, Springer, 2010.
- [85] J. Glaunes, A. Trouve, L. Younes, Diffeomorphic matching of distributions: a new approach for unlabelled point-sets and sub-manifolds matching, in: *Proceedings of the 2004 IEEE Computer Society Conference on Computer Vision and Pattern Recognition, CVPR 2004*, 2004.
- [86] S. Ardekani, A. Jain, S. Jain, T. Abraham, M. Abraham, S. Zimmerman, R. Winslow, M. Miller, L. Younes, Matching sparse sets of cardiac image cross-sections using large deformation diffeomorphic metric mapping algorithm, in: O. Camara, E. Konukoglu, M. Pop, K. Rhode, M. Sermesant, A. Young (Eds.), *Statistical Atlases and Computational Models of the Heart. Imaging and Modelling Challenges*, vol. 7085, Springer, Berlin, Heidelberg, 2012, pp. 234–243.
- [87] J.H. Seo, V. Vedula, T. Abraham, A. Lardo, F. Dawoud, H. Luo, R. Mittal, Effect of the mitral valve on diastolic flow patterns, *Phys. Fluids* 26 (12) (2014) 121901–1–121901–14.
- [88] B.E. Griffith, X. Luo, D.M. McQueen, C.S. Peskin, Simulating the fluid dynamics of natural and prosthetic heart valves using the immersed boundary method, *Int. J. Appl. Mech.* 1 (01) (2009) 137–177.
- [89] D.R. Einstein, K.S. Kunzelman, P.G. Reinhall, M. Nicosia, R. Cochran, Non-linear fluid-coupled computational model of the mitral valve, *J. Heart Valve Dis.* 14 (3) (2005) 376–385.
- [90] P. Watton, X. Luo, M. Yin, G. Bernacca, D. Wheatley, Effect of ventricle motion on the dynamic behaviour of chorded mitral valves, *J. Fluids Struct.* 24 (1) (2008) 58–74.

- [91] M. De Tullio, A. Cristallo, E. Balaras, R. Verzicco, Direct numerical simulation of the pulsatile flow through an aortic bileaflet mechanical heart valve, *J. Fluid Mech.* 622 (2009) 259–290.
- [92] M. De Tullio, J. Nam, G. Pascazio, E. Balaras, R. Verzicco, Computational prediction of mechanical hemolysis in aortic valved prostheses, *Eur. J. Mech. B, Fluids* 35 (2012) 47–53.
- [93] Y.J. Choi, V. Vedula, R. Mittal, Computational study of the dynamics of a bileaflet mechanical heart valve in the mitral position, *Ann. Biomed. Eng.* (2014) 1–13.
- [94] T.B. Le, F. Sotiropoulos, Fluid–structure interaction of an aortic heart valve prosthesis driven by an animated anatomic left ventricle, *J. Comput. Phys.* 244 (2013) 41–62.
- [95] M.-C. Hsu, D. Kamensky, Y. Bazilevs, M.S. Sacks, T.J. Hughes, Fluid–structure interaction analysis of bioprosthetic heart valves: significance of arterial wall deformation, *Comput. Mech.* 54 (4) (2014) 1055–1071.
- [96] E. Votta, T.B. Le, M. Stevanella, L. Fusini, E.G. Caiani, A. Redaelli, F. Sotiropoulos, Toward patient-specific simulations of cardiac valves: state-of-the-art and future directions, *J. Biomech.* 46 (2) (2013) 217–228.
- [97] F. Sotiropoulos, Fluid mechanics of heart valves and their replacements, *Annu. Rev. Fluid Mech.* 48 (1) (2015).
- [98] F. Domenichini, G. Pedrizzetti, Asymptotic model of fluid–tissue interaction for mitral valve dynamics, *Cardiovasc. Eng. Technol.* 6 (2) (2015) 95–104.
- [99] Y. Cheng, H. Oertel, T. Schenkel, Fluid–structure coupled CFD simulation of the left ventricular flow during diastole phase, *Ann. Biomed. Eng.* 33 (2005) 567–576.
- [100] T. Schenkel, M. Malve, M. Reik, M. Markl, B. Jung, H. Oertel, MRI-based CFD analysis of flow in a human left ventricle: methodology and application to a healthy heart, *Ann. Biomed. Eng.* 37 (3) (2009) 503–515.
- [101] J.W. Nichols, S.K. Lele, P. Moin, F.E. Ham, J.E. Bridges, Large-eddy simulation for supersonic rectangular jet noise prediction: effects of chevrons, *AIAA Pap.* 2212, 2012.
- [102] A.D. Paspoularides, M. Shu, M.S. Womack, A. Shah, O.V. Ramm, D.D. Glower, RV functional imaging: 3-D echo-derived dynamic geometry and flow field simulations, *Am. J. Physiol., Heart Circ. Physiol.* 284 (2003) H56–H65.
- [103] H. Watanabe, S. Sugiura, H. Kafuku, T. Hisada, Multiphysics simulation of left ventricular filling dynamics using fluid–structure interaction finite element method, *Biophys. J.* 87 (2004) 2074–2085.
- [104] W.K. Liu, Y. Liu, D. Farrell, L. Zhang, X.S. Wang, Y. Fukui, N. Patankar, Y. Zhang, C. Bajaj, J. Lee, et al., Immersed finite element method and its applications to biological systems, *Comput. Methods Appl. Mech. Eng.* 195 (13) (2006) 1722–1749.
- [105] C. Long, A. Marsden, Y. Bazilevs, Fluid–structure interaction simulation of pulsatile ventricular assist devices, *Comput. Mech.* 52 (5) (2013) 971–981.
- [106] R. Mittal, G. Iaccarino, Immersed boundary methods, *Annu. Rev. Fluid Mech.* 37 (2005) 239–261.
- [107] R. Mittal, H. Dong, M. Bozkurttas, F. Najjar, A. Vargas, A. von Loebbecke, A versatile sharp interface immersed boundary method for incompressible flows with complex boundaries, *J. Comput. Phys.* 227 (10) (2008) 4825–4852.
- [108] A.J. Chorin, On the convergence of discrete approximations to the Navier–Stokes equations, *Math. Comput.* 23 (106) (1969) 341–353.
- [109] W.H. Press, *Numerical Recipes: The Art of Scientific Computing*, 3rd edition, Cambridge University Press, 2007.
- [110] J. Zhou, R. Adrian, S. Balachandar, T. Kendall, Mechanisms for generating coherent packets of hairpin vortices in channel flow, *J. Fluid Mech.* 387 (1999) 353–396.
- [111] P. Chakraborty, S. Balachandar, R.J. Adrian, On the relationships between local vortex identification schemes, *J. Fluid Mech.* 535 (2005) 189–214.
- [112] N. Ranganathan, J. Lam, E. Wigle, M. Silver, Morphology of the human mitral valve II. The valve leaflets, *Circulation* 41 (3) (1970) 459–467.
- [113] D.J. Angiolillo, D. Capodanno, S. Goto, Platelet thrombin receptor antagonism and atherothrombosis, *Eur. Heart J.* (2009) ehp504.
- [114] J.H. Seo, R. Mittal, T. Abd, R. George, Coupled chemo-fluidic computational modeling of thrombogenesis in infarcted hearts, in: 4th International Conference on Computational and Mathematical Biomedical Engineering, CMBE2015, Cachan, France, 2015.
- [115] J. Biasseti, P.G. Spazzini, J. Swedenborg, T.C. Gasser, An integrated fluid–chemical model toward modeling the formation of intra-luminal thrombus in abdominal aortic aneurysms, *Front. Physiol.* 3 (2012).
- [116] K. Neeves, D. Illing, S. Diamond, Thrombin flux and wall shear rate regulate fibrin fiber deposition state during polymerization under flow, *Biophys. J.* 98 (7) (2010) 1344–1352.
- [117] K. Leiderman, A.L. Fogelson, Grow with the flow: a spatial–temporal model of platelet deposition and blood coagulation under flow, *Math. Med. Biol.* 28 (1) (2011) 47–84.
- [118] J.H. Seo, Y.J. Moon, Linearized perturbed compressible equations for low Mach number aeroacoustics, *J. Comput. Phys.* 218 (2) (2006) 702–719.
- [119] J.H. Seo, R. Mittal, A high-order immersed boundary method for acoustic wave scattering and low-Mach number flow-induced sound in complex geometries, *J. Comput. Phys.* 230 (4) (2011) 1000–1019.
- [120] H. Oung, F. Forsberg, Doppler ultrasound simulation model for pulsatile flow with nonaxial components, *Ultrason. Imag.* 18 (3) (1996) 157–172.
- [121] H. Liu, J.H. Seo, R. Mittal, H.H. Huang, GPU-accelerated scalable solver for banded linear systems, in: 2013 IEEE International Conference on Cluster Computing, CLUSTER, 2013.